CLASSIFYING PUMP-PROBE IMAGES OF MELANOCYTIC LESIONS USING THE WEYL TRANSFORM

Hyun Keun Ahn,[d] *Qiang Qiu,*[d] *Edward Bosch,*[m] *Andrew Thompson,*[o]
Francisco E. Robles,[g] *Guillermo Sapiro,*[d] *Warren S. Warren,*[d] *Robert Calderbank*[d]

[d] Duke University, Durham, NC 27707
[m] University of Maryland, College Park, MD 20742
[o] University of Oxford
[g] Georgia Institute of Technology College of Engineering, GA 30332

ABSTRACT

Diagnosis of melanoma is fraught with uncertainty, and discordance rates among physicians remain high because of the lack of a definitive criterion. Motivated by this challenge, this paper first introduces the Patch Weyl transform (PWT), a 2-dimensional variant of the Weyl transform. It then presents a method for classifying pump-probe images of melanocytic lesions based on the PWT coefficients. Performance of the PWT coefficients is shown to be superior to classification based on baseline intensity, on standard descriptors such as the Histogram of Oriented Gradients (HOG) and Local Binary Patterns (LBP), and on coefficients derived from PCA and Fourier representations of the data.

Index Terms— Image processing, Weyl transform, Convolution, Melanoma classification, Pump-probe images

1. INTRODUCTION

Melanoma is the fifth most common cancer in men and the seventh most common cancer in women in the United States [1]. In 2015, almost 74,000 people were diagnosed with invasive melanoma and nearly 10,000 people died from it [2]. Early detection of malignant melanoma is crucial in reducing the mortality rate [3]. Clinical diagnosis of melanoma is challenging mainly because many benign lesions have overlapping features with melanoma and no single criterion can be used to correctly classify the lesions.

Although histopathologic analysis and biopsy still remain the gold standards for diagnosis, interpretations vary among physicians themselves [4]; e,g., a study found a discordance rate of 14% [5]. False positive diagnosis occurs frequently; thus, patients are overburdened with increased medical costs and unnecessary melanoma treatments.

Because melanoma skin lesions are easily accessible, many optical imaging technologies have been utilized to capture possibly conclusive sets of features that may classify different stages of melanoma. It was recently found that the biochemical composition of melanin assessed with the pump-probe images of skin lesions is effective in distinguishing benign nevi from the melanoma [6]. However, it was not sufficient to classify different stages of melanoma.

The Weyl transform was introduced in [7] as a powerful method for capturing multiscale periodicity of image patches. In this paper, we propose implementation of the new variant of the Weyl transform, which we call the Patch Weyl transform, in the classification of the pump-probe images of the melanocytic lesions. We show empirically that the Patch Weyl transform coefficients perform much better in classification compared to pixel-averaged methods, standard descriptors such as LBP and HOG, and the coefficients derived from PCA and Fourier transform.

2. BACKGROUND

The following section provides necessary background information. Section 2.1 discusses the types of lesions explored in this paper. Section 2.2 explains the previous version of the Weyl transform.

2.1. Melanocytic Lesions

Benign melanocytic lesions, which include macule and nevi, often impede accurate diagnosis of melanoma. Macules are difficult to distinguish clinically from melanoma; nevi share many histological features with melanoma [8]. Melanoma is identified based on criterion such as increased melanocytic density, confluence, and atypia [9]. Hyperplasia currently has no clear definition; it typically shares one or two of the melanoma criterion above [9].

2.2. Weyl Transform

In [7], the Weyl coefficients were calculated from the trace inner products of the covariance matrix obtained from a vectorized patch of length 2^m with signed permutation matrices from the binary Heisenberg-Weyl group, denoted as $\{D(a,b)\}$, indexed by binary m-tuple $a = \{a_{m-1} \dots a_0\}^T \in \mathbb{Z}_2^m$ and $b = \{b_{m-1} \dots b_0\}^T \in \mathbb{Z}_2^m$, take the form

$$D(a,b) := (X^{a_{m-1}} Z^{b_{m-1}}) \otimes \dots \otimes (X^{a_0} Z^{b_0}),$$

where

$$X = \begin{bmatrix} 0 & 1 \\ 1 & 0 \end{bmatrix}, Z = \begin{bmatrix} 1 & 0 \\ 0 & -1 \end{bmatrix}.$$

Given a vectorized patch y, we define its Weyl coefficients $w_{a,b}(y)$ to be

$$w_{a,b}(y) := \frac{1}{2^{m/2}} Tr[yy^T \cdot D(a,b)].$$

3. METHODOLOGY

The data set consists of 637 images of melanocytic samples - hyperplasia (71), macule (119), melanoma (335) and nevi (112)-, each of size $420\mu m \times 420\mu m$, obtained from pump-probe microscopy of vulva-melanoma lesions, which provide a good starting point to test computational algorithms since these lesions tend to be highly pigmented and thus higher signal to noise ratio compared to skin lesions. Each image contains only one lesion. We randomly choose 50% of the images from each class as training and rest as testing.

3.1. Patch Weyl Transform

Here, we propose a variant of the Weyl transform used in [7] in which we replace the covariance matrix of a vectorized patch with the image patch itself. In the new Weyl transform, which we will refer to as the Patch Weyl transform (PWT), we write a patch P as the sum of symmetric $(P + P^T)/2$ and a skew-symmetric matrix $(P - P^T)/2$, so that it is specified by a pair of Hermitian matrices. Because Heisenberg-Weyl matrices form a basis for the real vector space of Hermitian matrices, a patch can be described by two sets of coefficients, which we define as symmetric or W_R and skew-symmetric or W_Q.

PWT turns out to be more scalable than the previous version in [7], which expands an image patch into a higher dimension, limiting the applicability of the transform to only very small patch sizes (e.g. 4×4 pixels). PWT, however, maintains the same dimension as the patch and thus is not limited by the size of the input. Any square patch of dimension 2^m, where $m \in \mathbb{N}$, is applicable.

PWT also retains some key properties of the original Weyl transform. Primarily, the PWT features detect periodicity. In addition, the magnitudes of the PWT coefficients are covariant under the group of transformation of the form $X \rightarrow \phi^* X \phi$, where the possible choices for ϕ correspond to elements of the binary Symplectic group.

Lastly, PWT allows convolution operation,

Classification	Base	HOG	LBP	PCA	Fourier	W$_R$	W$_Q$	W_R and W_Q
Melanoma VS Other	59%	65%	68%	70%	78%	96%	93%	94%
Macule VS Other	79%	80%	77%	86%	87%	99%	97%	98%
Nevi VS Other	74%	76%	75%	83%	90%	98%	95%	99%
Hyperplasia VS Other	76%	83%	85%	89%	89%	98%	97%	98%

Table 1: Classification accuracy achieved by the proposed Weyl Descriptors (W_R, W_Q, and both W_R and W_Q) compared to the baseline and other commonly used descriptors: HOG, LBP, PCA, Fourier.

which was not considered in [7]. For any two matrix A and B with same order, following equivalence between the trace product and Hadamard product holds: $Tr[A^T \cdot B] = \sum_{i,j}[A \circ B]_{ij}$. Computation of the PWT coefficients, which is a trace inner product, is essentially a convolution with $D(a,b)s$ as the filters. Thus, PWT application extends to a deep learning, such as convolutional neural networks.

3.2. Preprocessing

We preprocess the images to "concentrate" the salient regions of interest. Graph-based approach is adopted, where we construct a strongly connected graph G using pixel of the image as its node [10]. Then, we define Markov chain on G and compute its equilibrium distribution to find the most salient regions. Figure 1 shows the results of preprocessing.

3.3. Feature Selection

For each preprocessed pump-probe image, we extract the magnitudes of W_R and W_Q coefficients, each of which is returned as a square matrix, and vectorize them. Then from the training data sets, the top K W_R and W_Q coefficients for each lesion are selected using the following algorithm. Here is an example of selecting features from the W_R coefficients for classifying class c. We denote p and q to be the number of c images and of non-c images from the training sets, respectively. Let $W_{+,i}$ be the i^{th} column of the matrix W_+, where $W_{+,i} = W_R$ coefficients of the i^{th} c image. W_- is of similar matrix constructed from the non-c images. Let $Y = \frac{1}{pq}\sum_{i,j}|W_{+,i} - W_{-,j}|$. We rank

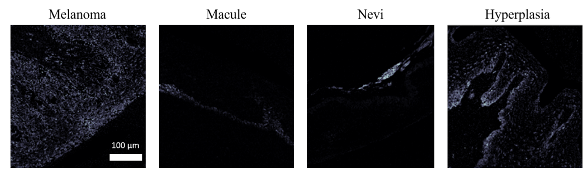

(a) Pump-probe images

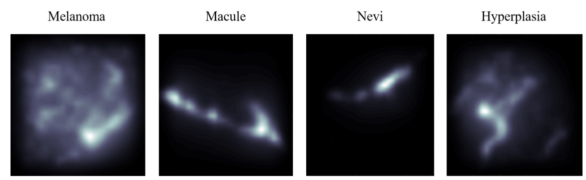

(b) Preprocessed pump-probe images

Fig. 1: Examples of images of different melanocytic samples.

the coefficients in descending order of Y. Same algorithm is applied to find the top K features for other class from PWT coefficients. From them, we generate three different feature vectors: (1) Top K W_R, (2) Top K W_Q, (3) Top K W_R and Top K W_Q, with total of 2K coefficients.

The unknown patch is assigned a label of its nearest neighbor training patch based on the Euclidean distance between them. Accuracy of the PWT coefficients is compared to the baseline intensity measures, HOG, LBP, Fourier, and PCA. Similar feature selection method is applied for the Fourier and PCA coefficients. For all of the experiments, the preprocessed images are used.

4. RESULTS

We perform One versus All analysis for each type of lesion. For each class, PWT descriptors outper-

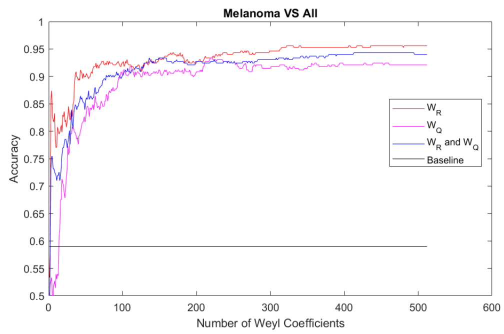

(a) Melanoma VS Others

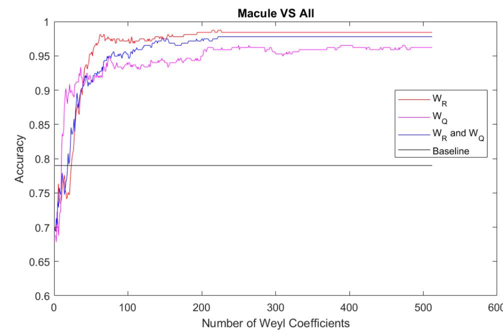

(b) Macule VS Others

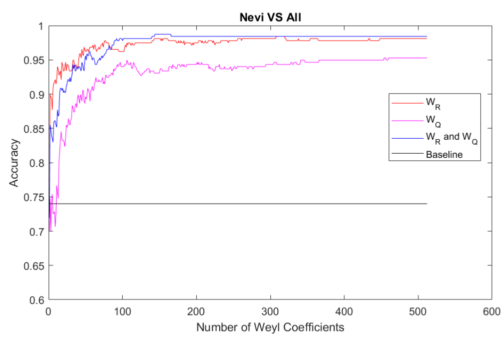

(c) Nevi VS Others

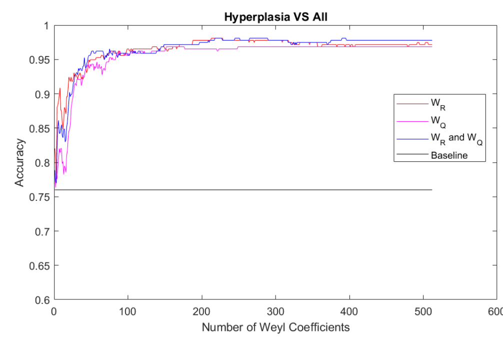

(d) Hyperplasia VS Others

Fig. 2: Classification accuracy of the PWT Descriptors for each type of melanocytic lesion. Each curve represents the different feature vectors used to represent the images.

form the baseline measure (Fig. 2). From the Table 1, we see that all forms of PWT feature vectors classify lesions much more accurately than the HOG and LBP, which performed relatively well in texture classification [7]. We also compared PWT features with the coefficients derived from PCA and Fourier transform, both of which involve generating the basis representation of the image, just as the Weyl transform generates the Heisenberg matrices which form the orthonormal basis of hermitian matrices [7]. PWT coefficients clearly outperform them (Table 1). Comparison of the performance of the W_R coefficients, which capture information on symmetry, and W_Q coefficients, which capture information on anti-symmetry, suggests that the symmetricity plays a bigger role in differentiating between lesion images. PWT descriptors may be potentially more useful and effective features to be applied in imaging analysis.

The results show that the PWT derived features, which provide information on periodicity and symmetry, perform well in the classification of the lesion images. Furthermore, we can reach the maximum accuracy after using approximately 100 coefficients for all sets of PWT descriptors. Since PWT is not limited by the size of the input data as the original Weyl transform, PWT is far more practical and diverse in application. Moreover, as discussed in section 3.1, PWT can be incorporated in deep learning architecture, such as the convolutional neural networks (CNNs), to learn much more complex characteristics of the data.

5. REFERENCES

[1] S. Azoury, J. Lange, and A. Jemal, "Epidemiology, Risk Factors, Prevention, and Early Detection of Melanoma," *Surgical Clinics of North America*, vol. 94, no. 5, pp. 945-962, 2014.

[2] R. Siegel, K. Miller, and A. Jemal, "Cancer Statistics," *CA Cancer J. Clinicians*, vol. 65, no. 1, pp. 5-29, 2015.

[3] D. S. Rigel, J. Russak, and R. Friedman. "The Evolution of Melanoma Diagnosis: 25 Years Beyond the ABCDs," *CA: A Cancer Journal for Clinicians*, vol. 60, no. 5, pp. 301-316, 2010.

[4] S. Patrawala, A. Maley, C. Greskovich, L. Stuart, D. Parker, R. Swerlick, and B. Stoff, "Discordance of Histopathologic Parameters in Cutaneous Melanoma: Clinical Implications," *Journal of the American Academy of Dermatology*, vol. 74, no. 1, pp. 75-78, 2016.

[5] B. A. Shoo, R. W. Sagebiel, and M. Kashani-Sabet, "Discordance in the histopathologic diagnosis of melanoma at a melanoma referral center," *J. Amer. Acad. Dermatology*, vol. 62, no. 5, pp. 751756, May 2010.

[6] T. E. Matthews, I. R. Piletic, M. A. Selim, M. J. Simpson, and W. S. Warren, "Pump-Probe Imaging Differentiates Melanoma from Melanocytic Nevi," *Science Translational Medicine*, vol. 3, no. 71, 2011.

[7] Q. Qiu, A. Thompson, R. Calderbank and G. Sapiro, "Data Representation using the Weyl Transform," *IEEE Transactions on Information Theory*, vol. 64, no. 7, pp. 1844–1853, 2016.

[8] G. Massi, P.E. LeBoit. Histological Diagnosis of Nevi and Melanoma. 2nd ed. New York: Springer; 2013.

[9] F.E. Robles, S. Deb, M.C. Fischer, W.S. Warren, M.A. Selim, (in press), Label-free imaging of female genital tract melanocytic lesions with pump-probe microscopy: A promising diagnostic tool, *Journal of Lower Genital Tract Disease*.

[10] J. Harel, C. Koch, and P. Perona, "Graph-Based Visual Saliency," *Advances in neural information processing systems*, pp. 545-552, 2006.